ARTICLE

Self-Assembly of Metal Oxides into Three-Dimensional Nanostructures: Synthesis and Application in Catalysis

Vivek Polshettiwar,* Babita Baruwati, and Rajender S. Varma*

Sustainable Technology Division, National Risk Management Research Laboratory, U.S. Environmental Protection Agency, 26 West M.L.K. Drive, MS 443, Cincinnati, Ohio 45268

ABSTRACT Nanostructured metal (Fe, Co, Mn, Cr, Mo) oxides were fabricated under microwave irradiation conditions in pure water without using any reducing or capping reagent. The metal oxides self-assembled into octahedra, spheres, triangular rods, pine, and hexagonal snowflake-like three-dimensional morphologies. Pine-structured nano-iron oxides were studied as a novel support for various catalytic organic transformations.

KEYWORDS: metal oxides · nanocatalyst · green organic transformations

The control over size and morphology of nanostructures to tailor the physical and chemical properties has become a fundamental issue in nanoscience. The development of solution-based controlled synthesis of nanomaterials has shaped a variety of dendritic hyperbranched structures.[1,2] Study of dendritic patterns in chemical synthesis has revealed that the distinctive dimensions, that is, size, shape, and chemical functionality, of such structures make them potential candidates for the design and invention of new functional nanomaterials.[3] Self-assembly of nanoparticles, such as nanoclusters, nanowires, nanobelts, and nanotubes,[1−3] is a modus operandi for designing novel sensors, circuits, and devices on the nano- and microscale.[4−6] Fractal structures are common in nature across all areas, from self-assembled molecules to the shapes of coastlines, to the distribution of galaxies, and to the shapes of clouds.[7]

After the study of semiconductor nanocrystallites by Brus *et al.*,[8] remarkable effort has been made to synthesize monodispersed nanocrystallites with quantum size effects.[9−15] Numerous efforts have been made for the synthesis of anisotropic nanostructures in liquid medium through hydrothermal processes,[16,17] in addition to physical and chemical vapor deposition approaches.[18,19] A variety of nanocrystalline chalcogenides,[20−27] metals,[28−30] and metal oxides[31,32] have been fabricated through precisely manipulating the reaction conditions. As a lean to this trend, many symmetric nanocrystals of noble metals,[33,34] copper oxides,[35] and sulfides[36] have also been synthesized. In recent years, extensive research has been performed on nanomaterials of various dimensions, which has led to substantial advances in nanomaterial synthesis.[37,38] In comparison with one-dimensional (1D), the three-dimensional (3D) nanostructures provide a great deal of opportunity to explore their novel properties. Also, the self-assembly of 1D structures into 3D structures *via* the solution-based route is becoming more attractive compared to the physical and chemical vapor deposition routes due to gentle synthesis conditions, ease of operation, and the possibility of large-scale production.

Microwave (MW) chemistry has been widely used in synthetic organic chemistry, with enhanced reaction rates, selectivity, and product yields.[39−43] This technique is also useful for the synthesis of high-quality nanomaterials *via* direct MW heating of the molecular precursors.[44−47] To the best of our knowledge, the hierarchical self-assembly of nanomaterials under MW irradiation has not been reported. However, after our initial success[48] and engaged in the development of greener and sustainable pathways for nanomaterials[48−53] and organic synthesis,[39−43] herein we report an easy and rapid synthesis of a variety of metal oxides having dendritic 3D nanostructures. In this work, the MW-assisted hydrothermal process was employed for the

*Address correspondence to polshettiwar.vivek@epa.gov, varma.rajender@epa.gov.

Received for review December 29, 2008 and accepted January 21, 2009.

Published online February 11, 2009.
10.1021/nn800903p CCC: $40.75

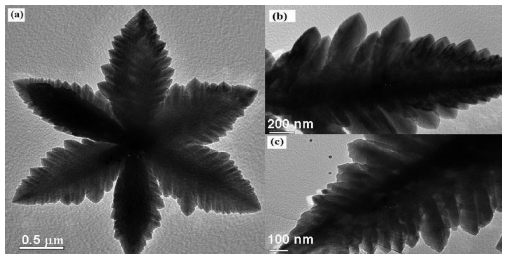

Figure 1. TEM of (a) snowflake and (b,c) pine α-Fe_2O_3.

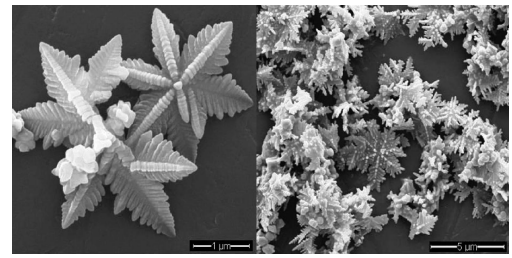

Figure 2. ESEM of dendritic α-Fe_2O_3.

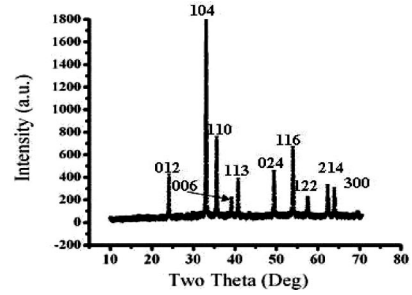

Figure 3. XRD of dendritic α-Fe_2O_3.

synthesis of dendritic metal oxides in water without using any reducing or capping reagent. The size and shape of the final product was tailored by varying substrate concentration and reaction temperature. Five different nanostructured metal (Fe, Mo, Co, Cr, and Mn) oxides of different morphologies were synthesized and characterized.

RESULTS AND DISCUSSION

The disadvantages of most of the known methods for the synthesis of these nano-oxides are the use of the surfactants, capping or reducing agents, and toxic organic solvents, which may limit their applications in terms of economical and environmental sustainability. In the present study, we emphasized the role of the metal hexacyano complex as a single precursor for the synthesis of these nanomaterials in pure water, without using any external reagents. Interestingly, these cyano complexes play a crucial role in the formation of well-defined 3D structures. However, if other metal sources such as metal chlorides, nitrates, or sulfates were used, even under similar reaction conditions, particles without any defined nanostructures were observed.

Five well-defined morphologies, including octahedron, spheres, triangular rods, pine, and hexagonal snowflake nanostructures, of metal oxides with sizes in the range of 100−500 nm have been obtained under MW irradiation conditions. Use of MW-assisted chemistry is due to the efficiency of the interaction of microwaves with water molecules[39,40,54] as well as with polar inorganic metal oxide precursors. The reaction mixture is rapidly heated to required temperatures under MW irradiation, and the precise control of the reaction temperature can be achieved because of the very high heat capacity of water.[54,55]

Fabrication of Iron Oxide (α-Fe_2O_3): Self-Assembly into Pine and Snowflake Nanostructures. α-Fe_2O_3 was synthesized using hydrothermal technique by simply heating the $K_4[Fe(CN)_6]$ in water under MW irradiation condition. During the reaction, $[Fe(CN)_6]^{4-}$ ion, having six equivalent cyanide atoms, dissociated in water, which in turn grew rapidly along its six crystallographical directions, yielding the α-Fe_2O_3 particles. The morphology of these particles appeared like a pine tree (Figures 1 and 2), hence the term micropine particle. TEM (Figure 1) and ESEM (Figure 2) images of the synthesized micropine α-Fe_2O_3 particles show the single-crystal structure. A closer inspection of these particles reveals well-defined and highly ordered branches (Figure 1b,c) distributed on both the sides. The TEM observations also revealed that the micropine dendrites self-assembled to form a sixfold snowflake-like structure (Figure 1a). Further structural characterization of this material was carried out using powder XRD (Figure 3), which shows α-Fe_2O_3 phase having a rhombohedral structure (JCPDS 01-089-0596). The diffraction peaks are sharp because of the crystalline nature of the particles. The crystallite size calculated from the Scherer formula using the full width at half-maximum (fwhm) of the most intense peaks was found to be 48.5 ± 1 nm.

Effect of Substrate Concentration and Reaction Temperature. The effects of substrate concentration and reaction temperature on the morphology of the nanoparticle were also studied. It was observed that, with an increase in the concentration, the sharpness of branched dendrite particles decreased and materials with slightly branched particles were formed (Figure 4). Reaction temperature plays a crucial role in this synthesis. At 150 °C, moderate to good product yields were obtained in 3 h; however, below this temperature, the formation of nanoparticles needed extended reaction time. Figure 4a−c shows TEM images of materials that were synthe-

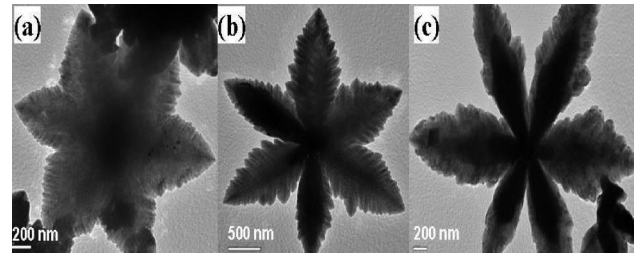

Figure 4. TEM of α-Fe_2O_3 particles using (a) 0.01, (b) 0.02, and (c) 0.03 mol of $K_4[Fe(CN)_6]$ at 150 °C under MW irradiation.

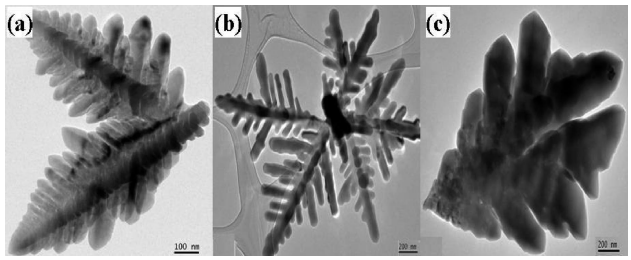

Figure 5. TEM of α-Fe_2O_3 particles using (a) 0.005, (b) 0.01, and (c) 0.05 mol of $K_4[Fe(CN)_6]$ at 180 °C under MW irradiation.

sized at $K_4[Fe(CN)_6]$ concentrations of 0.01, 0.02, and 0.03 mol, respectively, at 150 °C. The higher the concentration of $K_4[Fe(CN)_6]$, the thicker the nanorod branches of the dendrites. Broadening was also observed at higher reaction temperature (180 °C), depending on substrate concentration (Figure 5). These results suggest that it is possible to control and tune the shape of dendritic nanostructures by controlling the kinetic parameters (temperature and concentration) of the reaction process.

Fabrication of Cobalt Oxide (CoO): Self-Assembly into Octahedral Nanostructures. MW-assisted hydrothermal heating of $K_3[Co(CN)_6]$ in water fabricated cobalt oxide in good yield. TEM and SEM studies revealed the formation of octahedral nanoparticles with sizes ranging from 200 to 500 nm (Figure 6). For an octahedral crystal, every facet is close to an equilateral triangle. All the surfaces are smooth, and there are no defects. X-ray diffraction (XRD) of as-synthesized nanoparticles indicates the formation of cobalt oxide (Figure 7). The peaks could be indexed to the CoO phase of cobalt oxide having a cubic structure (JCPDS 03-065-2902). EDAX confirmed the presence of only cobalt and oxygen in the as-synthesized samples with an atomic ratio of 55 to 44, further confirming the phase of cobalt oxide. The crystallite size calculated from the Scherer formula using the fwhm of the most intense peaks was found to be 46.2 $\pm$ 1 nm. The effects of substrate concentration and reaction temperature on the morphology of the cobalt oxide nanoparticles were also studied; however, no significant changes were observed in the particle morphology.

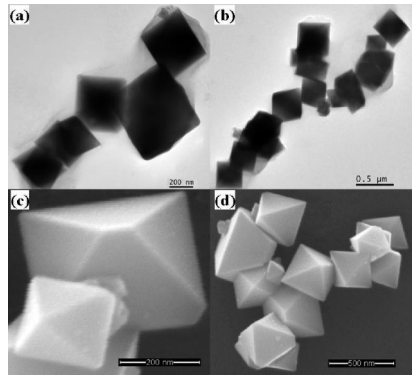

Figure 6. TEM (a,b) and ESEM (c,d) of cobalt oxide.

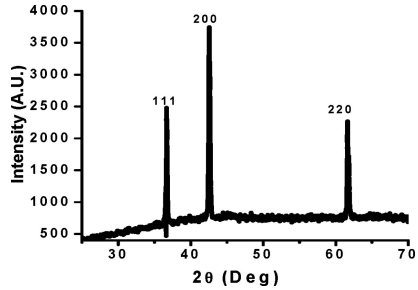

Figure 7. XRD of octahedral cobalt oxide.

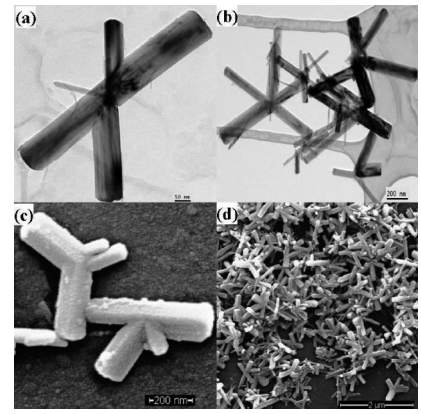

Figure 8. TEM (a,b) and ESEM (c,d) of manganese oxide.

Fabrication of Manganese Oxide (Mn_2O_3): Self-Assembly into Triangular Nanorods. Manganese oxide was also expeditiously synthesized by heating the aqueous solution of $K_3[Mn(CN)_6]$ under MW irradiation. TEM and SEM studies showed the formation of 3D nanoparticles with triangular rod morphology (Figure 8). These nanorods were approximately 100 nm in diameter with lengths

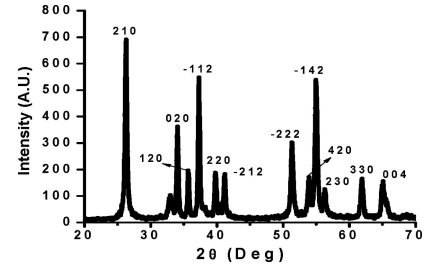

Figure 9. XRD of manganese oxide.

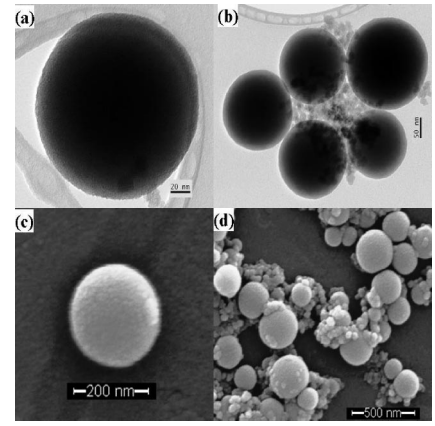

Figure 10. TEM (a,b) and ESEM (c,d) of chromium oxide.

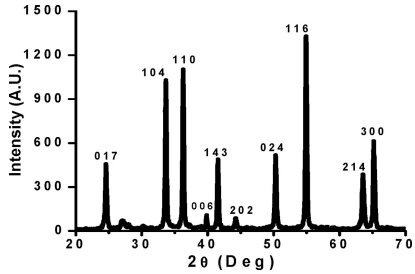

Figure 11. XRD of chromium oxide.

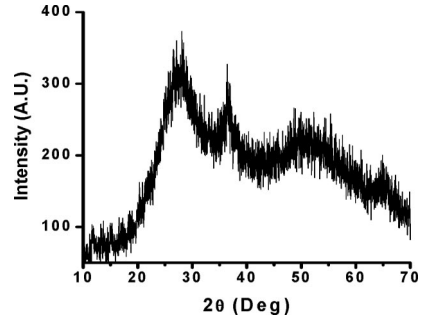

Figure 13. XRD of molybdenum oxide.

up to 500 nm. Although the morphologies of most of the nanoparticles were triangular rods, some small spherical nanoparticles were also observed in the case of higher precursor concentration reactions; this indicates that the formation of the triangular rods might be due to self-assembly of these small particles. A closer inspection of these particles revealed the further self-assembly of triangular rods into Y-shaped dendritic nanostructures (Figure 8). No effect of reaction temperature on the morphology of the manganese oxide nanoparticles was observed.

Further structural characterization of this material by powder XRD (Figure 9) indicates the formation of Mn_2O_3 phase of manganese oxide having orthorhombic structure (JCPDS 00-002-0429); sharp diffraction peaks are due to the crystalline nature of the nanoparticles. Crystallite size was calculated from the Scherer formula using the fwhm of the most intense peaks and was found to be 28.8 ± 2 nm.

Fabrication of Chromium Oxide (Cr_2O_3): Self-Assembly into Nanospheres. Chromium oxide was synthesized by irradiating the $K_3[Cr(CN)_6]$ solution using MW in the absence of reducing or capping agents. TEM micrographs (Figure 10a,b) show the dispersed spherical particles in the size range of 120−200 nm. However, SEM images (Figure 10c,d) show a large size distribution of the nanospheres, with particles ranging from 50 to 500 nm in size. The formation of larger particles may be due to Ostwald's ripening, wherein larger particles grow at the expense of the smaller particles. No significant variations in the particle size or morphology were noted when concentration of the precursors and reaction temperature were increased. The XRD pattern confirmed the phase of the as-synthesized nanoparticles to be Cr_2O_3 having a cubic structure (JCPDS 00-006-0504) (Figure 11). Crystallite size was calculated from the Scherer formula and was found to be 42.39 ± 2 nm.

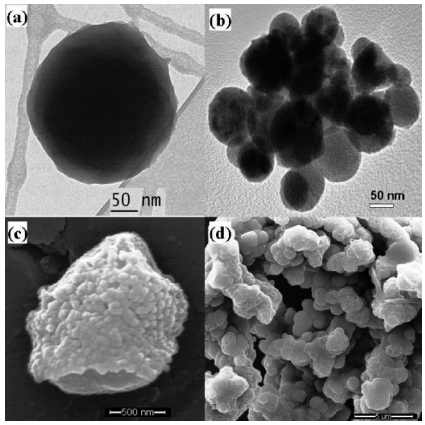

Figure 12. TEM (a,b) and ESEM (c,d) of molybdenum oxide.

Fabrication of Molybdenum Oxide (MoO_2): Self-Assembly into Nanospheres. Molybdenum oxide was also synthesized by irradiating the aqueous solution of $K_3[Mo(CN)_8]$ by microwaves without using any reducing or capping agents, and spherical nanoparticles were formed. From TEM and ESEM (Figure 12) micrographs, it can be seen that the particle sizes were ~200−250 nm. The XRD pattern confirmed the phase of the molybdenum oxides to be MoO_2 having a cubic structure, although the spectra were found to be highly broadened with very low signal-to-noise ratio (Figure 13). The EDAX also confirms the phase of the nanoparticles to be MoO_2 as the elements are present in 31 and 63 atomic percentage, respectively. The closer inspections of SEM micrographs revealed that the surfaces of these particles were rough, unlike other metal oxides formed.

Plausible Mechanism for the Formation of Nanostructured Materials. Dendritic fractals of numerous materials have been thoroughly investigated in the past.[56−60] It is well-established that fractal aggregation arises in situations far from thermodynamic equilibrium where high driving forces lead to the generation of crystallites and random self-assembly.[61] The model known as diffusion-limited aggregation (DLA) has been successfully developed to interpret this ramified growth of different systems controlled by diffusive processes.[62] In our system, all the used hexacyano precursors were very stable complexes and no reducing agent or base was present during the reaction, thus preventing the rapid formation of metal hydroxide. Moreover, the stability of

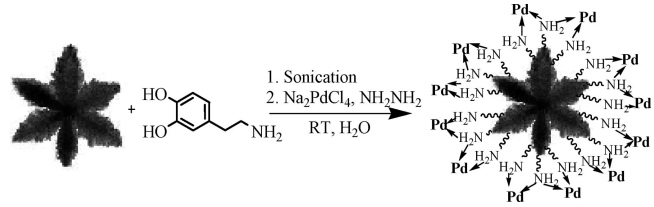

Scheme 1. Synthesis of functionalized ferrites with Pd coating.

TABLE 1. Suzuki Reaction of Aryl Halides Using Nano-Pd Catalyst

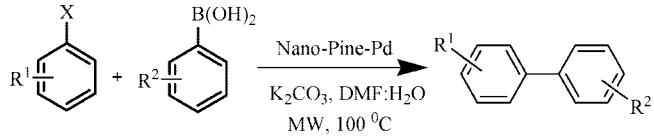

Entry	Halide	Boronic Acid	Product	Yields (%)
1	4-OMeC$_6$H$_5$Br	PhB(OH)$_2$	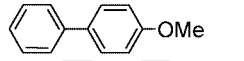	96
2	4-OMeC$_6$H$_5$Br	4-ClPhB(OH)$_2$	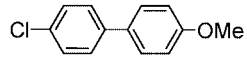	95
3	4-CHOC$_6$H$_5$Br	4-ClPhB(OH)$_2$	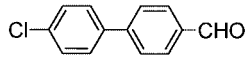	94
4	4-COMeC$_6$H$_5$Br	4-ClPhB(OH)$_2$	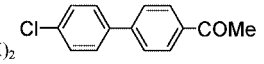	95
5	4-COMeC$_6$H$_5$Br	4-FPhB(OH)$_2$	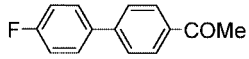	95
6	C$_6$H$_5$I	PhB(OH)$_2$	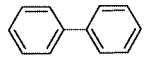	98
7	2-Iodothiophene	PhB(OH)$_2$	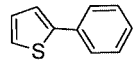	92

the precursor complexes can reduce the formation rate of free metal ions into the solution. At low concentration of free metal ions, the supersaturation is low, therefore, ions can combine to form nuclei. The slowly generated ions in the later stage have sufficient time for adsorption on those nuclei to form various nanostructures.

TABLE 2. Heck Reaction of Aryl Halides Using Nano-Pd Catalyst

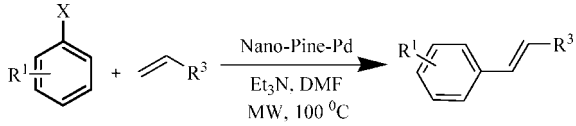

Entry	Aryl Halide	Product	Yield (%)
1	4-OMeC$_6$H$_5$Br	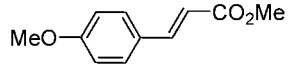	87
2.	4-OMeC$_6$H$_5$Br	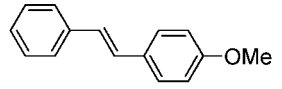	88
3	4-CHOC$_6$H$_5$Br	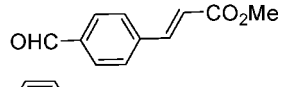	88
4	4-CHOC$_6$H$_5$Br	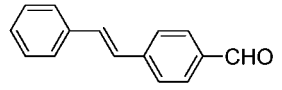	89
5	4-COMeC$_6$H$_5$Br	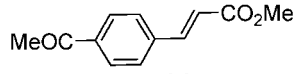	85
6	4-MeC$_6$H$_5$I	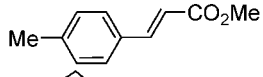	90
7	2-Iodothiophene	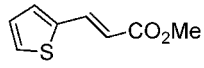	90

Nucleation and crystal growth are two imperative factors during the preparation of these nanostructured materials. In the cases of dendritic nanostructures, the ensuing morphology is conciliation between the inherent crystal structure of the material and the kinetic factors employed during the synthetic route. The preferred growth on certain planes becomes energetically favorable when the surface tensions of these planes are elevated and the bulk energy of the total system tends to decline.[63] The surface tensions of these planes possibly will be tuned to permit anisotropic growth by manipulating experimental conditions, such as substrate concentration, reaction temperature, and time. Other key factors affecting the morphology of these nano-oxides are the crystalline phases of seeds and subsequent growth. Crystal seeds can potentially have a variety of different crystallographic phases, and the stable phase is highly dependent on the environment.

$[Fe(CN)_6]^{4-}$ ions are very stable in aqueous solution, and the formation of pine-structured nanoferrite (α-Fe_2O_3) materials is based on the weak dissociation of these ions under MW-assisted hydrothermal conditions. These ions subsequently hydrolyze to form iron hydroxides, which in turn decompose into iron oxides and slowly grow along six crystallographically equivalent directions. The resulting structures display beautiful fractal features, which morphologically bear a resemblance to a pine tree. On similar lines, $K_3[Co(CN)_6]$ precursors, when dissolved in the water, started to decompose very slowly and smoothly under hydrothermal conditions so that the nuclei grew homogeneously. Aggregation of the cobalt oxide nuclei then formed small particles, which grew into octahedral nanostructures *via* an Ostwald ripening process.

In the cases of chromium and molybdenum oxides, formation of spherical nanostructures was observed. The crystallographic phase of the nucleated seeds might be the possible factor responsible for the formation of these spherical morphologies. Since the seed crystals of Cr_2O_3 and MoO_2 are in cubic phase, they tend to grow isotropically along the three crystallographic axes (*a*, *b*, and *c* directions), resulting in these shapes. However, in the case of manganese oxide, as the seeds are in an orthorhombic structure, crystals can grow anisotropically, resulting in shapes such as triangular rods.

Effect of Calcination over Morphology and Phase of Metal Oxides. The stability and effect of temperature on the morphology of the nanostructures was also studied. All the synthesized nanoparticles were calcinated at 700 °C for 2 h in air. Interestingly, the morphologies of iron oxide, manganese oxide, and chromium oxide remained unaltered even after calcinating at 700 °C. The phase of these nano-oxides also remained unchanged, indicating the high stability of materials. In the case of cobalt oxide (CoO) and molybdenum oxide (MoO_2), although the morphologies of the nanoparticles re-

TABLE 3. Sonogashira Reaction of Aryl Halides Using Nano-Pd Catalyst

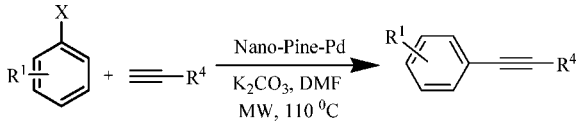

Entry	Aryl Halide	Product	Yield (%)
1	C_6H_5I	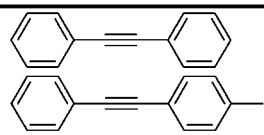	85
2	4-MeC_6H_5I		82
3	2-Iodothiophene	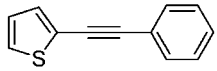	79
4	4-$COMeC_6H_5Br$	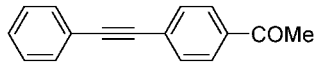	82
5	4-$OMeC_6H_5Br$	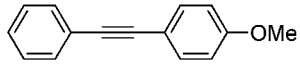	80
6	2-Iodothiophene	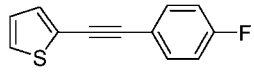	80
7	4-$OMeC_6H_5Br$	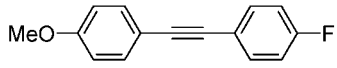	86

mained unchanged after calcination for 2 h, the phase of the particles changed to Co_3O_4 and MoO_3, respectively. This is an added advantage of our synthetic procedure, as the morphology of the nanometal oxides remains stable at high temperature even when associated with a phase change.

Nanoferrite as a Catalyst Support. In order to prove the utility of these materials, we tested synthesized nanoferrites as a support for heterogeneous catalysis. The first step was the functionalization of pine-tips of synthesized nanoferrites with an organic functional group, which will act as a ligand for metal-catalyzed reactions (Scheme 1). Catalyst was prepared by sonicating nanoparticles with dopamine followed by addition of palladium (Pd) salt at a basic pH. Material with Pd nanoparticles on the tips of amine-functionalized pine ferrites was obtained in excellent yield. FT-IR and XRD evidently confirmed the anchoring of dopamine and Pd particles on ferrite surfaces, and the weight percentage of Pd was found to be 7.26% by ICP-AES analysis.

The formation of carbon−carbon bonds *via* Pd-catalyzed cross-coupling reactions plays a crucial role in synthetic organic chemistry. Particular attention has been paid to the coupling reaction of aryl halides with boronic acids, alkenes, and alkynes, commonly called Suzuki, Heck, and Sonogashira reactions, respectively.[64,65] The practical use of the ever increasing number of tailor-made transition-metal catalytic species is indeed connected with the problem of separation and reuse of the rather costly catalyst systems. To overcome these problems, we explored this Pd-containing material as a heterogeneous catalyst for these coupling reactions and hydrogenation reactions (Tables 1−4).

Nanopine-Pd displayed high catalytic activity for Suzuki, Heck, Sonogashira, and hydrogenation reactions. All the reactions proceeded efficiently with good to excellent yields, with unchanged catalytic activity for at least five reaction cycles. For practical applications of heterogeneous systems, the lifetime of the catalyst and its level of reusability are very important factors. To clarify this issue, we established a set of experiments using the recycled catalyst. The catalyst also showed excellent recyclability in all the reactions. Heterogeneity and Pd leaching of this catalyst for the Heck reaction of iodobenzene and methyl acrylate were also examined by the modified "hot filtration" test. The reaction was stopped at 25% conversion, and the liquid reaction mixture was separated from solid nanocatalyst under hot conditions. The liquid portion, which was further subjected to MW irradiation, reacted only up to 30%, indicating negligible Pd leaching, which was further confirmed by ICP-AES analysis of the catalyst material before and after reactions.

CONCLUSIONS

We have developed a convenient synthetic protocol for metal oxides with 3D nanostructures under MW irradiation conditions. Materials were readily prepared from inexpensive starting materials in water without using any reducing or capping reagent. This economical and environmental sustainable synthetic concept could ultimately enable the fine-tuning of material responses to magnetic, electrical, optical, and mechanical stimuli. Five well-defined morphologies, including octahedron, spheres, triangular rods, pine, and hexagonal snowflake, with particles size in the range of 100−500 nm were obtained. Because of these unique morphologies, synthesized nanomaterials will have significant applications in biomedical science and catalysis. Nanoferrites

TABLE 4. Hydrogenation Reactions Using Nano-Pd Catalyst

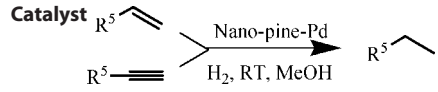

Entry	Substrate	Product	Yield (%)
1	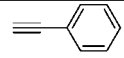	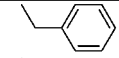	98
2	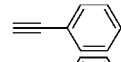	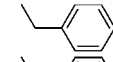	96
3	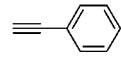	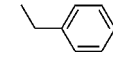	96
4	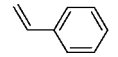	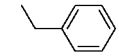	98
5	$CH_3(CH_2)_{11}CH{=}CH_2$	$CH_3(CH_2)_{11}CH_2CH_3$	98
6	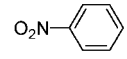	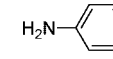	97

were then functionalized and coated with Pd metal, which catalyzed various C−C coupling and hydrogenation reactions with high yields. In addition, the effortless recovery and elevated efficiency, combined with the inherent stability of this catalyst, make the method sustainable.

METHODS

Synthesis of the Metal Oxides. In a typical synthetic procedure, 0.001 mol of the precursor $[K_4Fe(CN)_6$, $K_3Co(CN)_6$, $K_3Mn(CN)_6$, $K_3Mo(CN)_8$, and $K_3Cr(CN)_6]$ was dissolved in 50 mL of distilled water, and the solution was placed in a Teflon-sealed MW reactor. The reaction mixture was exposed to MW irradiation at 180 °C for 3 h. After completion of the reaction, mixture was allowed to cool to room temperature naturally and the metal oxides formed were isolated by centrifugation, washed with distilled water and methanol, and dried under a vacuum at 60 °C for 3−4 h.

Characterization. The phase of the as-synthesized metal oxide nanoparticles was determined by X-ray diffraction in an MMS X-ray diffractometer with a Cu Kα source in the 2θ range of 10 to 70. The data were collected with a step of 1 deg/min. A few drops of the as-synthesized nanoparticles in isopropanol were added to a quartz plate and dried at room temperature before recording the X-ray pattern. TEM micrographs were recorded on a Phillips CM 20 TEM microscope at an operating voltage of 200 kV. A drop of the as-synthesized nanoparticles in ethanol was loaded on a carbon-coated copper grid and then allowed to dry at room temperature before recording the micrographs. The SEM images were recorded on a FEI/Phillips XL 30 ESEM-FEG instrument coupled with electron dispersive X-ray analysis (EDAX). To obtain a better SEM image, the product was coated with thin layer of gold on the surface to make it conducting.

Synthesis of Nanopine-Pd Catalyst. Amine-functionalized α-Fe_2O_3 nanoparticles (1 g) were dispersed in water, and $NaPdCl_4$ solution in water was added to the mixture to get 10 wt % of Pd. Hydrazine monohydrate solution in water was added dropwise to bring the pH of this mixture to 9. The reaction mixture was then stirred for 24 h at room temperature. The product was allowed to settle, washed several times with water and acetone, and dried under vacuum at 60 °C for 2 h (80% yield). The weight percentage of Pd in the catalyst was found to be 7.26% by ICP-AES analysis.

Experimental for Suzuki Reactions. The aryl halide (1 mmol), boronic acid (1.2 mmol), K_2CO_3 (1.5 mmol), and 50 mg of nanopine-Pd catalyst were added to 2 mL of DMF/H_2O (1:1) in a 10 mL crimp-sealed thick-walled glass tube equipped with a pressure sensor and a magnetic stirrer. The reaction tube was then placed inside the cavity of a CEM Discover focused MW synthesis system, operated at 100 ± 5 °C (temperature monitored by a built-in infrared sensor), power 200 W (maximum), and pressure 50 psi (maximum) for 20 min. After completion of the reaction, the reaction mixture was decanted to separate nanomaterials and crude product. All products (Table 1) are known in the literature and were identified by comparing their MS spectra with Wiley library.

Experimental for Heck Reactions. The aryl halide (1 mmol), alkene (1.2 mmol), triethylamine (1.5 mmol), and 0.1 g of nanopine-Pd catalyst were added to 2 mL of DMF in a 10 mL crimp-sealed thick-walled glass tube, and the above procedure was followed at 100 ± 5 °C for 30 min. All products (Table 2) are known in the literature and were identified by comparing their MS spectra with standard Wiley library.

Experimental for Sonogashira Reactions. The aryl halide (1 mmol), alkyne (1.2 mmol), K_2CO_3 (1.5 mmol), and 0.1 g of nanopine-Pd catalyst were added to 2 mL of DMF in a 10 mL crimp-sealed thick-walled glass tube, and the above procedure was followed at 110 ± 5 °C for 45 min. All products (Table 3) are known in the literature and were identified by comparing their MS spectra with standard Wiley library.

Experimental for Hydrogenation Reactions. To a solution of alkynes/alkenes/nitro compounds (1 mmol) in 2 mL of methanol was added 10 mg of nanopine-Pd catalyst. The reaction vessel was purged three times with hydrogen and charged to 40 psi, and then closed off to the source of hydrogen. The reaction was stirred for 2 h at room temperature. After completion of the reaction, the reaction mixture was decanted to separate nanomaterials and crude product. All products (Table 4) are known in the literature and were identified by comparing their MS spectra with standard Wiley library.

Acknowledgment. V.P. and B.B. are postgraduate research participants at the National Risk Management Research Laboratory, EPA, administered by the Oak Ridge Institute for Science and Education.

REFERENCES AND NOTES

1. Sun, S.; Murray, C. B; Weller, D.; Folks, L.; Moser, A. Monodisperse FePt Nanoparticles and Ferromagnetic FePt Nanocrystal Superlattices. *Science* **2000**, *287*, 1979–1982.
2. Moore, J. S.; Kraft, M. L. Chemistry: Synchronized Self-Assembly. *Science* **2008**, *320*, 620–621.
3. Shevchenko, E. V.; Talapin, D. V.; Kotov, N. A.; O'Brien, S.; Murray, C. B. Structural Diversity in Binary Nanoparticle Superlattices. *Nature* **2006**, *439*, 55–59.
4. Didiot, C.; Pons, S.; Kierren, B.; Fagot-Revurat, Y.; Malterre, D. Nanopatterning the Electronic Properties of Gold Surfaces with Self-organized Superlattices of Metallic Nanostructures. *Nat. Nanotechnol.* **2007**, *2*, 617–621.
5. Redl, F. X.; Cho, K. S.; Murray, C. B.; O'Brien, S. Three-Dimensional Binary Superlattices of Magnetic Nanocrystals and Semiconductor Quantum Dot. *Nature* **2003**, *423*, 968–971.
6. Joachim, C.; Gimzewski, J. K.; Aviram, A. Electronics Using Hybrid-Molecular and Mono-Molecular Devices. *Nature* **2000**, *408*, 541–548.
7. Klug, A. From Macromolecules to Biological Assemblies. *Angew. Chem., Int. Ed. Engl.* **1983**, *22*, 565–582.
8. Brus, L. E. Electron−Electron and Electron−Hole Interactions in Small Semiconductor Crystallites: The Size Dependence of the Lowest Excited Electronic State. *J. Chem. Phys.* **1984**, *80*, 4403–4409.
9. Kortan, A. R.; Hull, R.; Opila, R. L.; Bawendi, M. G.; Steigerwald, M. L.; Carroll, P. J.; Brus, L. E. Nucleation and Growth of Cadmium Selendie on Zinc Sulfide Quantum Crystallite Seeds, and *Vice Versa*, in Inverse Micelle Media. *J. Am. Chem. Soc.* **1990**, *112*, 1327–1332.
10. Wang, Y.; Herron, N. Nanometer-Sized Semiconductor Clusters: Materials Synthesis, Quantum Size Effects, and Photophysical Properties. *J. Phys. Chem.* **1991**, *95*, 525–532.
11. Murray, C. B.; Norris, D. J.; Bawendi, M. G. Synthesis and Characterization of Nearly Monodisperse CdE (E = Sulfur, Selenium, Tellurium) Semiconductor Nanocrystallites. *J. Am. Chem. Soc.* **1993**, *115*, 8706–8715.
12. Peng, X. G.; Wickham, J.; Alivisatos, A. P. Kinetics of II−VI and III−V Colloidal Semiconductor Nanocrystal Growth: "Focusing" of Size Distributions. *J. Am. Chem. Soc.* **1998**, *120*, 5343–5344.
13. Peng, Z. A.; Peng, X. G. Formation of High-Quality CdTe, CdSe, and CdS Nanocrystals Using CdO as Precursor. *J. Am. Chem. Soc.* **2001**, *123*, 183–184.
14. Wang, X.; Zhuang, J.; Peng, Q.; Li, Y. D. A General Strategy for Nanocrystal Synthesis. *Nature* **2005**, *437*, 121–124.
15. Cao, Y. C.; Wang, J. H. One-Pot Synthesis of High-Quality Zinc-Blende CdS Nanocrystals. *J. Am. Chem. Soc.* **2004**, *126*, 14336–14337.
16. Li, R. F.; Luo, Z. T.; Papadimitrakopoulos, F. Redox-Assisted Asymmetric Ostwald Ripening of CdSe Dots to Rods. *J. Am. Chem. Soc.* **2006**, *128*, 6280–6281.
17. Peng, X.; Manna, L.; Yang, W.; Wickham, J.; Scher, E.; Kadavanich, A.; Alivisatos, A. P. Shape Control of CdSe Nanocrystals. *Nature* **2000**, *404*, 59–61.

18. Nanda, K. K.; Sahu, S. N. One-Dimensional Quantum Confinement in Electrodeposited PbS Nanocrystalline Semiconductors. *Adv. Mater.* **2001**, *13*, 280–283.
19. Iijima, S. Helical Microtubules of Graphitic Carbon. *Nature* **1991**, *354*, 56–58.
20. Yong, K. T.; Sahoo, Y.; Swihart, M. T.; Prasad, P. N. Growth of CdSe Quantum Rods and Multipods Seeded by Noble-Metal Nanoparticles. *Adv. Mater.* **2006**, *18*, 1978–1982.
21. Milliron, D. J.; Hughes, S. M.; Cui, Y.; Manna, L.; Li, J. B.; Wang, L. W.; Alivisatos, A. P. Colloidal Nanocrystal Heterostructures with Linear and Branched Topology. *Nature* **2004**, *430*, 190–195.
22. Xu, L.; Zhang, W.; Ding, Y.; Yu, W.; Xing, J.; Li, F.; Qian, Y. Shape-Controlled Synthesis of PbS Microcrystals in Large Yields *via* A Solvothermal Process. *J. Cryst. Growth* **2004**, *273*, 213–219.
23. Manna, L.; Milliron, D. J.; Meisel, A.; Scher, E. C.; Alivisatos, A. P. Controlled Growth of Tetrapod-Branched Inorganic Nanocrystals. *Nat. Mater.* **2003**, *2*, 382–385.
24. Lifshitz, E.; Bashouti, M.; Kloper, V.; Kigel, A.; Eisen, M. S.; Berger, S. Synthesis and Characterization of PbSe Quantum Wires, Multipods, Quantum Rods, and Cubes. *Nano Lett.* **2003**, *3*, 857–862.
25. Lee, S. M.; Jun, Y. W.; Cho, S. N.; Cheon, J. Single-Crystalline Star-Shaped Nanocrystals and Their Evolution: Programming the Geometry of Nano-Building Blocks. *J. Am. Chem. Soc.* **2002**, *124*, 11244–11245.
26. Jun, Y. W.; Lee, S. M.; Kang, N. J.; Cheon, J. Controlled Synthesis of Multi-Armed CdS Nanorod Architectures Using Monosurfactant System. *J. Am. Chem. Soc.* **2001**, *123*, 5150–5151.
27. Manna, L.; Scher, E. C.; Alivisatos, A. P. Synthesis of Soluble and Processable Rod, Arrow, Teardrop, and Tetrapod-Shaped CdSe Nanocrystals. *J. Am. Chem. Soc.* **2000**, *122*, 12700–12706.
28. Zettsu, N.; McLellan, J. M.; Wiley, B; Yin, Y; Li, Z. Y.; Xia, Y. Synthesis, Stability, and Surface Plasmonic Properties of Rhodium Multipods, and their Use as Substrates for Surface-Enhanced Raman Scattering. *Angew. Chem., Int. Ed.* **2006**, *45*, 1288–1292.
29. Teng, X.; Yang, H. Synthesis of Platinum Multipods: An Induced Anisotropic Growth. *Nano Lett.* **2005**, *5*, 885–891.
30. Hoefelmeyer, J. D.; Niesz, K.; Somorjai, G. A.; Tilley, T. D. Radial Anisotropic Growth of Rhodium Nanoparticles. *Nano Lett.* **2005**, *5*, 435–438.
31. Ould-Ely, T.; Prieto-Centurion, D.; Kumar, A.; Guo, W.; Knowles, W. V.; Asokan, S.; Wong, M. S.; Rusakova, I.; Luttge, A.; Whitmire, K. H. Manganese(II) Oxide Nanohexapods: Insight into Controlling the Form of Nanocrystals. *Chem. Mater.* **2006**, *18*, 1821–1829.
32. Zitoun, D.; Pinna, N.; Frolet, N.; Belin, C. Single Crystal Manganese Oxide Multipods by Oriented Attachment. *J. Am. Chem. Soc.* **2005**, *127*, 15034–15035.
33. Seo, D.; Park, J. C.; Song, H. Polyhedral Gold Nanocrystals with O_h Symmetry: From Octahedra to Cubes. *J. Am. Chem. Soc.* **2006**, *128*, 14863–14870.
34. Sun, Y. G.; Xia, Y. N. Shape-Controlled Synthesis of Gold and Silver Nanoparticles. *Science* **2002**, *298*, 2176–2179.
35. Gou, L. F.; Murphy, C. J. Solution-Phase Synthesis of Cu_2O Nanocubes. *Nano Lett.* **2003**, *3*, 231–234.
36. Cao, H. L.; Qian, X. F.; Wang, C.; Ma, X. D.; Yin, J.; Zhu, Z. K. High Symmetric 18-Facet Polyhedron Nanocrystals of Cu_7S_4 with a Hollow Nanocage. *J. Am. Chem. Soc.* **2005**, *127*, 16024–16025.
37. Son, S. J.; Reichel, J.; He, B.; Schuchman, M.; Lee, S. B. Magnetic Nanotubes for Magnetic-Field-Assisted Bioseparation, Biointeraction, and Drug Delivery. *J. Am. Chem. Soc.* **2005**, *127*, 7316–7317.
38. Cao, G. *Nanostructures and Nanomaterials: Synthesis, Properties and Applications*; Imperial College Press: London, 2004; 433pp (ISBN 1-86094-415-9).
39. Polshettiwar, V.; Varma, R. S. Aqueous Microwave Chemistry: A Clean and Green Synthetic Tool for Rapid Drug Discovery. *Chem. Soc. Rev.* **2008**, *37*, 1546–1557.
40. Polshettiwar, V.; Varma, R. S. Microwave-Assisted Organic Synthesis and Transformations Using Benign Reaction Media. *Acc. Chem. Res.* **2008**, *41*, 629–639.
41. Polshettiwar, V.; Varma, R. S. Greener and Sustainable Approaches to the Synthesis of Pharmaceutically Active Heterocycles. *Curr. Opin. Drug Discovery Dev.* **2007**, *10*, 723–737.
42. Polshettiwar, V.; Varma, R. S. Olefin Ring Closing Metathesis and Hydrosilylation Reaction in Aqueous Medium by Grubbs Second Generation Ruthenium Catalyst. *J. Org. Chem.* **2008**, *73*, 7417–7419.
43. Polshettiwar, V.; Varma, R. S. Tandem Bis-Aldol Reaction of Ketones: A Facile One-Pot Synthesis of 1,3-Dioxanes in Aqueous Medium. *J. Org. Chem.* **2007**, *72*, 7420–7422.
44. Gerbec, J. A.; Magana, D.; Washington, A.; Strouse, G. F. Microwave-Enhanced Reaction Rates for Nanoparticle Synthesis. *J. Am. Chem. Soc.* **2005**, *127*, 15791–15800.
45. Sommer, W. J.; Weck, M. Facile Functionalization of Gold Nanoparticles *via* Microwave-Assisted 1,3 Dipolar Cycloaddition. *Langmuir* **2007**, *23*, 11991–11995.
46. Gao, F.; Lu, Q.; Komarneni, S. Interface Reaction for The Self-Assembly of Silver Nanocrystals under Microwave-Assisted Solvothermal Condition. *Chem. Mater.* **2005**, *17*, 856–860.
47. Hu, X.; Yu, J. C.; Gong, J. Fast Production of Self-Assembled Hierarchical α-Fe_2O_3 Nanoarchitectures. *J. Phys. Chem. C* **2007**, *111*, 11180–11185.
48. Polshettiwar, V.; Nadagouda, M. N.; Varma, R. S. The Synthesis and Applications of a Micro-Pine-Structured Nanocatalyst. *Chem. Commun.* **2008**, 6318–6320.
49. Nadagouda, M. N.; Polshettiwar, V.; Varma, R. S. Self-Assembly of Palladium Nanoparticles: Synthesis of Nanobelts, Nanoplates and Nanotrees Using Vitamin B1 and Their Application in Carbon−Carbon Coupling Reactions. *J. Mat. Chem.* **2009**, *19*, doi: 10.1039/b817112b.
50. Polshettiwar, V.; Varma R. S. Nanoparticle-Supported and Magnetically Recoverable Ruthenium Hydroxide Catalyst: Efficient Hydration of Nitriles to Amides in Aqueous Medium. *Chem.—Eur. J.* **2009**, *15*, 1582−1586.
51. Polshettiwar, V.; Varma, R. S. Nanoparticle-Supported and Magnetically Recoverable Palladium (Pd) Catalyst: A Selective and Sustainable Oxidation Protocol with High Turnover Number. *Org. Bio. Chem.* **2009**, *7*, 37–40.
52. Polshettiwar, V.; Baruwati, B.; Varma, R. S. Nanoparticle-Supported and Magnetically Recoverable Nickel Catalyst: A Robust and Economic Hydrogenation and Transfer Hydrogenation Protocol. *Green. Chem.* **2009**, *11*, 127−131.
53. Baruwati, B.; Nadagouda, M. N.; Varma, R. S. Bulk Synthesis of Monodisperse Ferrite Nanoparticles at Water-Organic Interfaces under Conventional and Microwave Hydrothermal Treatment and their Surface Functionalization. *J. Phys. Chem. C* **2008**, *112*, 18399–18404.
54. Dallinger, D.; Kappe, C. O. Microwave-Assisted Synthesis in Water as Solvent. *Chem. Rev.* **2007**, *107*, 2563–2591.
55. Li, C. J.; Chen, L. Organic Chemistry in Water. *Chem. Soc. Rev.* **2006**, *35*, 68–82.
56. Tian, Z. G. R.; Liu, J.; Voigt, J. A.; Xu, H. F.; Mcdermott, M. J. Dendritic Growth of Cubically Ordered Nanoporous Materials through Self-Assembly. *Nano Lett.* **2003**, *3*, 89–92.
57. Peng, Q.; Dong, Y. J.; Deng, Z. X.; Li, Y. D. Selective Synthesis and Characterization of CdSe Nanorods and Fractal Nanocrystals. *Inorg. Chem.* **2002**, *41*, 5249–5254.
58. Wang, X. Q.; Naka, K.; Itoh, H.; Park, S.; Chujo, Y. Synthesis of Silver Dendritic Nanostructures Protected by Tetrathiafulvalene. *Chem. Commun.* **2002**, 1300–1301.
59. Xiao, J. P.; Xie, Y.; Tang, R.; Chen, M.; Tian, X. B. Novel Ultrasonically Assisted Templated Synthesis of Palladium and Silver Dendritic Nanostructures. *Adv. Mater.* **2001**, *13*, 1887–1891.
60. Zhou, Y. S.; Yu, H.; Wang, C. Y.; Li, X. G.; Zhu, Y. R.; Chen, Z. Y. A Novel Ultraviolet Irradiation Photoreduction Technique for the Preparation of Single-Crystal Ag

Nanorods and Ag Dendrites. *Adv. Mater.* **1999**, *11*, 850–852.
61. Wang, M.; Liu, X. Y.; Strom, C. S.; Bennema, P.; Enckevort, W.; Ming, N. B. Fractal Aggregations at Low Driving Force with Strong Anisotropy. *Phys. Rev. Lett.* **1998**, *80*, 3089–3092.
62. Brady, R. R.; Ball, R. C. Fractal Growth of Copper Electrodeposits. *Nature* **1984**, *309*, 225–229.
63. Zhang, K. Q. *In Situ* Observation of Colloidal Monolayer Nucleation Driven by an Alternating Electric Field. *Nature* **2004**, *429*, 739–743.
64. Polshettiwar, V.; Molnar, A. Silica-Supported Pd Catalysts for Heck Coupling Reactions. *Tetrahedron* **2007**, *63*, 6949–6976.
65. Yin, L.; Liebscher, J. Carbon-Carbon Coupling Reactions Catalyzed by Heterogeneous Palladium Catalysts. *Chem. Rev.* **2007**, *107*, 133–173.